Available online at www.sciencedirect.com
ScienceDirect
Journal of Sound and Vibration 301 (2007) 319–340
JOURNAL OF SOUND AND VIBRATION
www.elsevier.com/locate/jsvi

Topology optimization problems for reflection and dissipation of elastic waves

Jakob S. Jensen

Department of Mechanical Engineering, Solid Mechanics, Technical University of Denmark, Nils Koppels Allé, Building 404, DK-2800 Kgs. Lyngby, Denmark

Received 29 August 2006; received in revised form 11 October 2006; accepted 11 October 2006
Available online 28 November 2006

Abstract

This paper is devoted to topology optimization problems for elastic wave propagation. The objective of the study is to maximize the reflection or the dissipation in a finite slab of material for pressure and shear waves in a range of frequencies. The optimized designs consist of two or three material phases: a host material and scattering and/or absorbing inclusions. The capabilities of the optimization algorithm are demonstrated with two numerical examples in which the reflection and dissipation of ground-borne wave pulses are maximized.

1. Introduction

This work deals with two fundamental optimization problems encountered in the study of elastic wave propagation through a finite slab of material. Wave propagation can be suppressed if the wave reflection or the wave dissipation is maximized and in this work these two problems are addressed with the method of topology optimization. The method is used to find an optimized distribution of inclusions of scattering and/or absorbing material that maximizes the reflection and/or the dissipation, respectively.

Recently, much work has been devoted to highly reflecting materials and structures created with a periodic distribution of scattering inclusions—the so-called bandgap materials. If inclusions are distributed periodically a large reflection of propagating waves can occur due to destructive interference. For a comprehensive overview see e.g. the recent review paper by Sigalas et al. [1].

Bandgap structures are promising candidates as optimal wave reflecting structures. In Sigmund and Jensen [2] it was demonstrated that optimized designs are typically periodic-like structures with modifications near the boundaries that compensate for edge effects. A material optimization problem was also considered in which the topology of repetitive identical inclusions was optimized. Rupp et al. [3] studied similar problems with a topology optimization algorithm. Halkjær et al. [4] considered bending waves in beams and plates and structures with limited spatial dimensions that did not allow for a repetitive periodic structure. Hussein et al. [5] analyzed one-dimensional wave propagation through a layered medium and used a genetic algorithm to generate optimized structures.

E-mail address: jsj@mek.dtu.dk.

0022-460X/$ - see front matter
doi:10.1016/j.jsv.2006.10.004

Optimization of the dissipation of elastic waves has been far less studied than the reflection/transmission problem. Planar structures that maximize dissipation of scalar waves was previously demonstrated by the author [6]. Razansky et al. [7] studied dissipation of acoustic waves and gave bounds for maximal dissipation in thin and thick dissipative layers. Work has also been done on optimal placement of dampers to reduce structural dynamic compliance [8,9]. Related work with the method topology optimization were seen in Jog [10] who studied the forced vibration problem and minimized the dissipated energy and in Wang and Chen [11] who maximized heat dissipation in cellular structures.

Closely related to this present work are optimization studies related to propagation of electromagnetic waves. Cox and Dobson [12] studied optimal design of infinite periodic structures with a material distribution method and maximized the optic (photonic) bandgaps and Jensen and Sigmund [13] studied a finite photonic bandgap structure and topology optimized the material distribution in a 90° bend so that the transmitted power through the bend was maximized.

This paper extends the work of Jensen [6] and considers dissipation of elastic waves (pressure and shear) for multiple frequencies instead of scalar waves at a single frequency. The work of Halkjær et al. [4] is extended to deal with the multiple frequency case. Furthermore, both optimization problems are extended to allow for the distribution of three material phases instead of two. The paper is organized as follows: first, the general model for elastic wave propagation is presented (Section 2), and the formulation of the two optimization problems are discussed in detail (Section 3). Section 4 describes the parametrization of the design domain with two continuous design fields, the material interpolation model, and the artificial damping penalization. In Section 5 the numerical implementation of the optimization problem is explained, including boundary conditions, FEM discretization, and a mathematical formulation of the problem. In Sections 6 and 7 two numerical examples are presented that demonstrate optimization of the material distribution for maximized reflection and dissipation of ground-borne wave pulses. Finally, main conclusions are given in Section 8.

2. Elastodynamic model

The computational model is based on the full 3D elastodynamic equations for an inhomogeneous medium. The 3D model is reduced to a 2D model under the assumption that the waves propagate in the plane and material properties vary in the same plane.

The 3D elastodynamic equations:

$$\rho\ddot{\mathbf{U}} = \boldsymbol{\nabla}\cdot\boldsymbol{\Sigma}, \tag{1}$$

govern the displacements $\mathbf{U} = \{U(\mathbf{x},t)\ V(\mathbf{x},t)\ W(\mathbf{x},t)\}^{\mathrm{T}}$ of an elastic medium with position-dependent density $\rho = \rho(\mathbf{x})$. The position vector is denoted $\mathbf{x} = \{x\ y\ z\}^{\mathrm{T}}$, and $\boldsymbol{\Sigma} = \boldsymbol{\Sigma}(\mathbf{x},t)$ is the stress tensor.

Eq. (1) is transformed to complex form with the complex variable transformation $\mathbf{U} \to \tilde{\mathbf{U}}$ and $\boldsymbol{\Sigma} \to \tilde{\boldsymbol{\Sigma}}$, so that $\mathbf{U} = \mathrm{Re}(\tilde{\mathbf{U}})$ and $\boldsymbol{\Sigma} = \mathrm{Re}(\tilde{\boldsymbol{\Sigma}})$. Time-harmonic motion with frequency ω gives a steady-state solution to the complex version of Eq. (1):

$$\tilde{\mathbf{U}}(\mathbf{x},t) = \mathbf{u}(\mathbf{x})\mathrm{e}^{\mathrm{i}\omega t}, \tag{2}$$

$$\tilde{\boldsymbol{\Sigma}}(\mathbf{x},t) = \boldsymbol{\sigma}(\mathbf{x})\mathrm{e}^{\mathrm{i}\omega t}, \tag{3}$$

in which the displacement amplitude vector $\mathbf{u}(\mathbf{x})$ and the stress amplitude tensor $\boldsymbol{\sigma}(\mathbf{x})$ are generally complex. The solution forms (2) and (3) are inserted into the complex version of Eq. (1) to give the standard time-harmonic elastic wave equation:

$$\boldsymbol{\nabla}\cdot\boldsymbol{\sigma} + \rho\omega^2\mathbf{u} = 0. \tag{4}$$

With the appropriate boundary conditions Eq. (4) gives the displacement field used as the basis for the optimization problems introduced in the following section. With a specific solution to the complex equation (4) the instantaneous displacement and stresses are:

$$\mathbf{U}(\mathbf{x},t) = \mathrm{Re}(\mathbf{u}(\mathbf{x})\mathrm{e}^{\mathrm{i}\omega t}) = \mathbf{u}^r\cos\omega t - \mathbf{u}^i\sin\omega t, \tag{5}$$

$$\mathbf{\Sigma}(\mathbf{x},t) = \mathrm{Re}(\boldsymbol{\sigma}(\mathbf{x})\mathrm{e}^{\mathrm{i}\omega t}) = \boldsymbol{\sigma}^r \cos\,\omega t - \boldsymbol{\sigma}^i \sin\omega t, \tag{6}$$

where superscripts r and i refer to the real and imaginary parts of the complex variable.

Eq. (4) is simplified by assuming the stresses to be invariant in a single direction (arbitrarily chosen as the z-direction) and can be written in component form as:

$$\frac{\partial\sigma_{xx}}{\partial x} + \frac{\partial\sigma_{yx}}{\partial y} + \rho\omega^2 u = 0, \tag{7}$$

$$\frac{\partial\sigma_{xy}}{\partial x} + \frac{\partial\sigma_{yy}}{\partial y} + \rho\omega^2 v = 0, \tag{8}$$

$$\frac{\partial\sigma_{xz}}{\partial x} + \frac{\partial\sigma_{yz}}{\partial y} + \rho\omega^2 w = 0, \tag{9}$$

with $\mathbf{u} = \{u(\mathbf{x})\ v(\mathbf{x})\ w(\mathbf{x})\}^{\mathrm{T}}$. This assumption could be realized, e.g. with a uniform material distribution in the z-direction and waves that propagate strictly in the (x,y)-plane.

For a linear isotropic elastic medium the stress components are:

$$\sigma_{xx} = \frac{E}{(1+\nu)(1-2\nu)}\left((1-\nu)\frac{\partial u}{\partial x} + \nu\frac{\partial v}{\partial y}\right), \tag{10}$$

$$\sigma_{xy} = \sigma_{yx} = \frac{E}{2(1+\nu)}\left(\frac{\partial u}{\partial y} + \frac{\partial v}{\partial x}\right), \tag{11}$$

$$\sigma_{yy} = \frac{E}{(1+\nu)(1-2\nu)}\left((1-\nu)\frac{\partial v}{\partial y} + \nu\frac{\partial u}{\partial x}\right), \tag{12}$$

for the coupled in-plane problem, and

$$\sigma_{xz} = \frac{E}{2(1+\nu)}\frac{\partial w}{\partial x}, \tag{13}$$

$$\sigma_{yz} = \frac{E}{2(1+\nu)}\frac{\partial w}{\partial y}, \tag{14}$$

for the scalar out-of-plane problem. In the following the coupled problem will be considered. Various optimization results for the out-of-plane problem can be found e.g. in Refs. [2,6].

3. Optimization problems

Two optimization problems are considered in this paper. The basic setup is displayed in Fig. 1. A plane elastic wave propagates in a loss-free host material. Within the slab of material, indicated by the vertical dashed lines, a number of scattering and/or absorbing inclusions cause the incident wave to be partially reflected and/or possibly dissipated and partially transmitted through the slab. The power balance for the system is

$$\tilde{I} = \tilde{R} + \tilde{T} + \tilde{D}, \tag{15}$$

where $\tilde{I}$ is the incident wave power, $\tilde{T}$ and $\tilde{R}$ is the transmitted and reflected power, respectively, and $\tilde{D}$ is the power dissipated due to absorbing inclusions.

3.1. Maximizing reflection

The first optimization problem is to maximize the reflection of the propagating wave with an optimized distribution of inclusions of one or two scattering materials. Pressure and shear waves at multiple frequencies are treated but the analysis is restricted to plane waves with normal incidence.

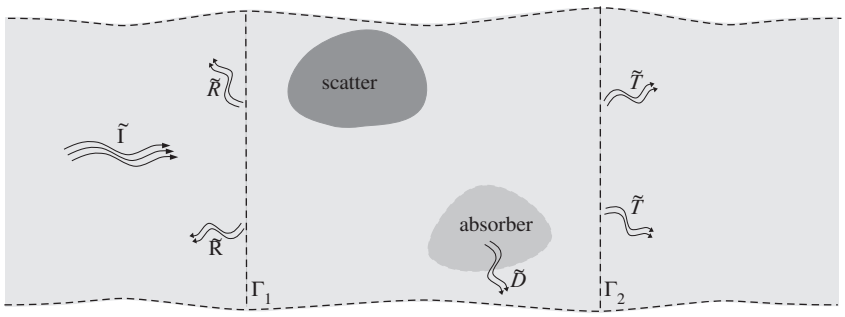

Fig. 1. Basic setup for the two optimization problems. Incident wave power is denoted $\tilde{I}$, transmitted and reflected power $\tilde{T}$ and $\tilde{R}$, and the dissipated power is $\tilde{D}$.

The reflection of the wave is found indirectly from the transmitted power at the output boundary Γ_2. The instantaneous transmitted power (Poynting vector) is defined as (e.g. Ref. [14, p. 133]):

$$\mathbf{p}(\mathbf{x},t) = \{p_x(\mathbf{x},t) \;\; p_y(\mathbf{x},t)\}^{\mathrm{T}}, \tag{16}$$

where

$$p_x(\mathbf{x},t) = -\Sigma_{xx}\dot{U} - \Sigma_{yx}\dot{V}, \tag{17}$$

$$p_y(\mathbf{x},t) = -\Sigma_{xy}\dot{U} - \Sigma_{yy}\dot{V}, \tag{18}$$

is the power in the x- and y-direction, respectively.

Expressions for $\dot{\mathbf{U}}$ and $\boldsymbol{\Sigma}$, taken from Eqs. (5)–(6), are inserted into Eqs. (17)–(18) so that p_x and p_y are expressed in terms of the computed quantities $\mathbf{u}$ and $\boldsymbol{\sigma}$. Now, the time-averaged x- and y-components of the power can be computed as:

$$\langle p_x(\mathbf{x},t)\rangle = \frac{\omega}{2\pi}\int_0^{2\pi/\omega} (-\Sigma_{xx}\dot{U} - \Sigma_{yx}\dot{V})\,\mathrm{d}t = \tfrac{1}{2}\omega\mathrm{Re}(\mathrm{i}\sigma_{xx}\bar{u} + \mathrm{i}\sigma_{yx}\bar{v}), \tag{19}$$

$$\langle p_y(\mathbf{x},t)\rangle = \frac{\omega}{2\pi}\int_0^{2\pi/\omega} (-\Sigma_{xy}\dot{U} - \Sigma_{yy}\dot{V})\,\mathrm{d}t = \tfrac{1}{2}\omega\mathrm{Re}(\mathrm{i}\sigma_{xy}\bar{u} + \mathrm{i}\sigma_{yy}\bar{v}), \tag{20}$$

where the notation $\langle\,\rangle = \omega/2\pi\int_0^{2\pi/\omega}\mathrm{d}t$ is introduced and will be used in the following. In Eqs. (19)–(20) the overbar denotes complex conjugation. The time-averaged power $\tilde{T}$ transmitted through the output boundary is now found as:

$$\tilde{T} = \left\langle \int_{\Gamma_2} \mathbf{n}\cdot\mathbf{p}\,\mathrm{d}\mathbf{x} \right\rangle = \int_{\Gamma_2} \langle p_x\rangle\,\mathrm{d}\mathbf{x}, \tag{21}$$

in which $\mathbf{n} = \{1\;0\}^{\mathrm{T}}$ is the outward pointing normal vector at Γ_2.

Without dissipation the reflected power $\tilde{R}$ is simply the difference between the time-averaged incident and transmitted power $\tilde{R} = \tilde{I} - \tilde{T}$ and the corresponding reflectance R is computed by scaling $\tilde{R}$ with $\tilde{I}$:

$$R = \frac{\tilde{I} - \tilde{T}}{\tilde{I}} = 1 - T, \tag{22}$$

where $T = \tilde{T}/\tilde{I}$ is the transmittance and $\tilde{I}$ is found by evaluating the Poynting vector at the input boundary Γ_1:

$$\tilde{I}_p = \int_{\Gamma_1} \langle -\dot{U}\Sigma_{xx}\rangle\,\mathrm{d}\mathbf{x}, \tag{23}$$

for a plane pressure (P) wave of normal incidence (pure horizontal motion) and

$$\tilde{I}_s = \int_{\Gamma_1} \langle -\dot{V}\Sigma_{yx} \rangle \, \mathrm{d}\mathbf{x}, \tag{24}$$

for shear (S) wave (vertical motion). In Section 5 a set of boundary conditions are specified that ensure a unit magnitude incident wave that propagates away from Γ_1 in both directions. Eqs. (23)–(24) are evaluated with these boundary conditions (Eqs. (49)–(50)):

$$\tilde{I} = \tfrac{1}{2} h \omega^2 Z, \tag{25}$$

where h is the vertical dimension of the input boundary and Z is the wave impedance, given as $Z = Z_p$ for a P wave and $Z = Z_s$ for an S wave, in which:

$$Z_p = \sqrt{\frac{E_h \rho_h (1 - \nu_h)}{(1 + \nu_h)(1 - 2\nu_h)}}, \tag{26}$$

$$Z_s = \sqrt{\frac{E_h \rho_h}{2(1 + \nu_h)}}, \tag{27}$$

and the subscript h denotes host material which is fixed at the boundary Γ_1. Thus, the final expression for the reflectance from the slab of material between Γ_1 and Γ_2 is

$$R = 1 - \frac{1}{h\omega Z} \int_{\Gamma_2} \mathrm{Re}(\mathrm{i}\sigma_{xx}\bar{u} + \mathrm{i}\sigma_{yx}\bar{v}) \mathrm{d}\mathbf{x}, \tag{28}$$

that takes the value 1 when the wave is fully reflected and 0 with full transmission. The reflectance R will be the first objective function in the optimization study.

3.2. Maximizing dissipation

An alternative optimization problem is now defined. Another way to hinder propagation of the wave is to maximize the dissipation of the wave within the slab. A benefit of this is that potential annoyance associated with the reflected wave can be eliminated.

Naturally, the dissipation of the wave energy is dependent on the damping model. A simple model is mass- and stiffness-proportional viscous damping. Reasonable agreement with experimental results can be obtained in large frequency ranges if a suitable combination of these two contributions are used. In this work smaller frequency ranges are considered and a simple mass-proportional damping model is chosen.

The mass-proportional viscous damping is added directly to the continuous Eq. (1):

$$\rho \ddot{\mathbf{U}} + \rho \eta_\rho \dot{\mathbf{U}} = \boldsymbol{\nabla} \cdot \boldsymbol{\Sigma}, \tag{29}$$

where $\eta_\rho = \eta_\rho(\mathbf{x})$ is a position-dependent damping coefficient. Eq. (29) leads to a time-harmonic wave equation with a complex density:

$$\boldsymbol{\nabla} \cdot \boldsymbol{\sigma} + \tilde{\rho}\omega^2 \mathbf{u} = 0, \tag{30}$$

$$\tilde{\rho} = \rho\left(1 - \mathrm{i}\frac{\eta_\rho}{\omega}\right). \tag{31}$$

A power balance is obtained by multiplying both sides of Eq. (29) by the velocities:

$$\dot{\mathbf{U}} \cdot (\rho \ddot{\mathbf{U}}) + \dot{\mathbf{U}} \cdot (\rho \eta_\rho \dot{\mathbf{U}}) = \dot{\mathbf{U}} \cdot (\boldsymbol{\nabla} \cdot \boldsymbol{\Sigma}). \tag{32}$$

The second term on the l.h.s. is the instantaneous point-wise dissipated power:

$$d(\mathbf{x}, t) = \rho \eta_\rho \dot{\mathbf{U}} \cdot \dot{\mathbf{U}}, \tag{33}$$

which averaged over a wave period yields the time-averaged dissipation:

$$\langle d(\mathbf{x},t)\rangle = \tfrac{1}{2}\omega^2\rho\eta_\rho(u\bar{u}+v\bar{v}). \tag{34}$$

The second objective function $\tilde{D}$ is defined as the time-averaged dissipation $\langle d(\mathbf{x},t)\rangle$ integrated over the total domain Ω. The relative dissipation D is obtained by scaling with the input power $\tilde{I}$:

$$D = \frac{\tilde{D}}{\tilde{I}} = \frac{1}{hZ}\int_\Omega \rho\eta_\rho(u\bar{u}+v\bar{v})\,\mathrm{d}\mathbf{x}. \tag{35}$$

4. Design variables and material interpolation

The design optimization is based on two continuous design fields ϱ_1 and ϱ_2 that are defined everywhere within the slab:

$$\varrho_1(\mathbf{x}) \in \mathbb{R}|\ 0 \leqslant \varrho_1 \leqslant 1, \tag{36}$$

$$\varrho_2(\mathbf{x}) \in \mathbb{R}|\ 0 \leqslant \varrho_2 \leqslant 1. \tag{37}$$

These two design fields are used to specify and control the point-wise material properties and can, in the present formulation, be used to distribute three different materials in the slab. For both problems one material is the host material through which the undisturbed wave propagates and the other two may be scattering and/or absorbing materials.

Any material property; E, ρ, ν or η_ρ is found by a linear interpolation between the properties of the involved materials:

$$\alpha(\mathbf{x}) = (1-\varrho_1)\alpha_h + \varrho_1((1-\varrho_2)\alpha_1 + \varrho_2\alpha_2), \tag{38}$$

in which α is any of the properties. Subscript h denotes host material, and subscripts 1 and 2 refer to the two other materials. A material interpolation scheme such as Eq. (38) is a standard implementation for three-phase design. See e.g. Bendsøe and Sigmund [15, p. 120], for a similar implementation with two materials and void.

From Eq. (38) it can be seen that the design field ϱ_1 is an indicator of host material (obtained for $\varrho_1 = 0$) or inclusion (obtained for $\varrho_1 = 1$). If an inclusion is specified by ϱ_1, the field ϱ_2 then specifies the inclusion type. Hence, type 1 is found for $\varrho_2 = 0$ ($\varrho_1 = 1$) and type 2 for $\varrho_2 = 1$ ($\varrho_1 = 1$). Non $0-1$ values of the design variables correspond to some intermediate material property that may not be physically realizable. This is not important in the optimization procedure, but it must be ensured that only $0-1$ values remain in the finalized optimized design so that the material properties are well defined.

4.1. Penalization with artificial dissipation

In most implementations of material interpolation models, penalization factors are introduced (SIMP model) (e.g. Ref. [15, p. 5]). This is done so that the continuous design variables are likely to take only the extreme values 0 or 1 in the final design. The SIMP strategy is not used in this work since a constraint on the amount of one of the material phases is required and for this problem such a constraint is not natural. Moreover, previous studies on wave propagation problems have shown that maximum material contrasts are favored so that $0-1$ optimized designs appear automatically [12,2,4]. However, in the dissipation example intermediate design variables appear especially with three material phases. In this case a penalization method is adapted that was originally introduced for optics problems.

In Jensen and Sigmund [16] it was suggested to use artificial damping to penalize intermediate design variables. An extra damping term was introduced:

$$\eta_{\mathrm{art}} = \beta\varrho(1-\varrho), \tag{39}$$

for the case of a single design field ϱ. In Eq. (39) β is a damping coefficient and the product $\varrho(1-\varrho)$ ensures that only intermediate design variables cause dissipation of energy. This penalization is similar to the explicit penalization method introduced by Allaire and Francford [17]. A nice physical interpretation is possible by imagining the intermediate material as a sponge that soaks up energy.

Here, this approach is reused and expanded to deal with two design fields:

$$\eta_{\text{art}} = \beta_1 \varrho_1((1-\varrho_1) + \beta_2 \varrho_2(1-\varrho_2)), \tag{40}$$

where the two factors β_1 and β_2 allow for separate penalization of ϱ_1 and ϱ_2 (in the numerical examples $\beta_2 = 1$). The specific form of Eq. (40) is connected to the definition of the design fields, i.e. if $\varrho_1 = 0$ host material is obtained regardless of the value of ϱ_2. Thus, only if $\varrho_1 \neq 0$ intermediate values of ϱ_2 should be penalized. The fraction of the input power that is dissipated due to the artificial damping is

$$D_{\text{art}} = \frac{\beta_1}{hZ} \int_\Omega \rho \varrho_1((1-\varrho_1) + \beta_2 \varrho_2(1-\varrho_2))(u\bar{u} + v\bar{v})\,\mathrm{d}\mathbf{x}. \tag{41}$$

where ρ is given from Eq. (38).

It should be emphasized that the artificial damping approach penalizes intermediate design variables only if the optimization problem is of the maximization type. With a minimization problem, e.g. minimizing the reflection, a work-around could be either to reformulate the problem into a maximization problem (e.g. maximizing the transmission) or alternatively to use a negative artificial damping coefficient β_1. The latter approach, however, lacks an appealing physical interpretation and has not been thoroughly tested.

5. Numerical implementation

The computational model is shown in Fig. 2. The design domain is defined with outer dimensions $L \times h$, input boundary Γ_1 at $x = 0$, and output boundary Γ_2 at $x = L + 2\delta$. Two perfectly matched layers (PMLs) are added to the computational domain to absorb waves propagating away from the design domain (at arbitrary angles) in the positive and/or negative x-direction, respectively. The reader is referred to Basu and Chopra [18] for a comprehensive treatment of PMLs for elastic waves.

5.1. Perfectly matched layers (PML)

PMLs generally ensure a low reflection for all angles of incidence for pressure and shear waves. A good performance of the absorbing boundary is important since the distribution of inclusions is not known a priori and a good optimization algorithm can be expected to exploit this. The good performance comes, however, at the expense of increased computational requirements due to the enlarged domain.

For the computational model in Fig. 2, the governing equations in the PMLs become:

$$\frac{1}{\varepsilon}\frac{\partial \tilde{\sigma}_{xx}}{\partial x} + \frac{\partial \tilde{\sigma}_{yx}}{\partial y} + \rho_h \omega^2 u = 0, \tag{42}$$

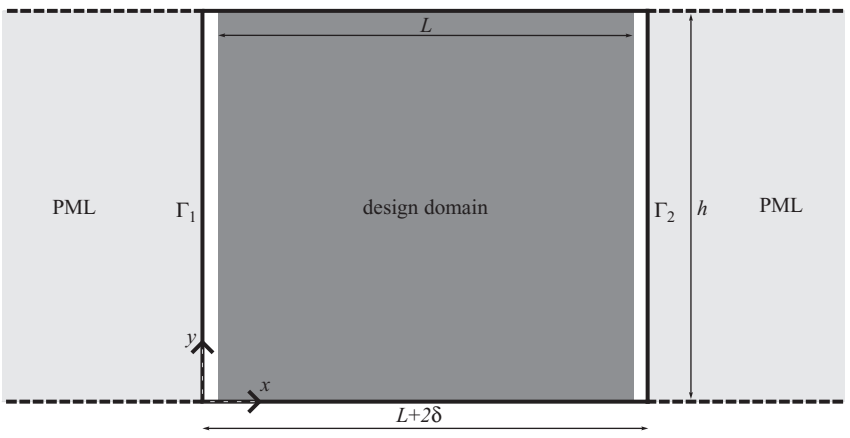

Fig. 2. Computational model used for numerical implementation of the optimization algorithm.

$$\frac{1}{\varepsilon}\frac{\partial \tilde{\sigma}_{xy}}{\partial x}+\frac{\partial \tilde{\sigma}_{yy}}{\partial y}+\rho_h\omega^2 v=0, \tag{43}$$

where the modified stress components are:

$$\tilde{\sigma}_{xx}=\frac{E_h}{(1+\nu_h)(1-2\nu_h)}\left(\frac{1}{\varepsilon}(1-\nu_h)\frac{\partial u}{\partial x}+\nu_h\frac{\partial v}{\partial y}\right), \tag{44}$$

$$\tilde{\sigma}_{xy}=\tilde{\sigma}_{yx}=\frac{E_h}{2(1+\nu_h)}\left(\frac{1}{\varepsilon}\frac{\partial v}{\partial x}+\frac{\partial u}{\partial y}\right), \tag{45}$$

$$\tilde{\sigma}_{yy}=\frac{E_h}{(1+\nu_h)(1-2\nu_h)}\left((1-\nu_h)\frac{\partial v}{\partial y}+\frac{1}{\varepsilon}\nu_h\frac{\partial u}{\partial x}\right), \tag{46}$$

in which subscript h indicates that the material in the PMLs is host material. The complex variable ε is a function of x:

$$\varepsilon(x)=1-\mathrm{i}\alpha\left(\frac{x-x^*}{L^*}\right)^2, \tag{47}$$

where x^* is the x-position of PML layer/real domain interface, and α is the absorption coefficient in the layer. The total length of the PML domain is L^*. Eq. (47) fulfills that $\varepsilon=1$ for $x=x^*$, so that the PML equations (42)–(43) reduce to the normal wave equations at the interface. The imaginary part of ε ensures the dissipation of the wave. The choice of letting the imaginary part increase with square of the distance from the interface is empirical but has been shown to yield low reflection values [18]. The coefficient α should be chosen large enough so that the wave is fully absorbed in the PMLs, but not excessively large so that spurious reflections occur at the interface. Here, $L^*=L/2$ and $\alpha=50$ have been used in the numerical examples.

5.2. Boundary conditions

A non-zero stress amplitude jump at Γ_1 specifies a stress wave propagating away from the boundary in both directions:

$$\mathbf{n}\cdot(\boldsymbol{\sigma}^+-\boldsymbol{\sigma}^-)=2\mathrm{i}\omega\{Z_pU_0 \quad Z_sV_0\}^{\mathrm{T}}, \tag{48}$$

where $\mathbf{n}=\{-1\ 0\}^{\mathrm{T}}$ is the normal vector pointing away from Ω, $(\boldsymbol{\sigma}^+-\boldsymbol{\sigma}^-)$ is the stress jump and U_0 and V_0 are the amplitudes of the P and S wave. Thus for a P wave of unit magnitude:

$$-(\sigma_{xx}^+-\sigma_{xx}^-)=2\mathrm{i}\omega Z_p, \tag{49}$$

and

$$-(\sigma_{xy}^+-\sigma_{xy}^-)=2\mathrm{i}\omega Z_s, \tag{50}$$

gives a unit magnitude S wave that propagates away from Γ_1.

The wave input boundary condition and the transition to the PMLs are simplified with constant material properties (host material) at the interface. This is accomplished by moving the design domain a small distance δ (Fig. 2) away from Γ_1 and Γ_2 . The transmitted power is averaged over the small domain instead of evaluated at the boundary:

$$T=\frac{1}{h\omega Z\delta}\int_{L+\delta}^{L+2\delta}\int_0^h \mathrm{Re}(\mathrm{i}\sigma_{xx}\bar{u}+\mathrm{i}\sigma_{yx}\bar{v})\,\mathrm{d}y\,\mathrm{d}x, \tag{51}$$

as this simplifies the numerical implementation of the sensitivities (Section 5.3).

A periodic boundary condition is applied for the amplitude fields on the upper boundary:

$$\mathbf{u}(x,h)=\mathbf{u}(x,0), \tag{52}$$

as well as zero traction conditions at the outer PML boundaries.

5.3. FEM discretization and sensitivity analysis

The commercial finite element software package COMSOL is used to discretize the domain and to assemble and solve the discretized equations. The two displacement fields u, v as well as the two design fields ϱ_1 and ϱ_2 are discretized as follows:

$$u(\mathbf{x}) = \sum_{i=1}^{N} \psi_i^1 u_i, \quad v(\mathbf{x}) = \sum_{i=1}^{N} \psi_i^2 v_i, \tag{53}$$

$$\varrho_1(\mathbf{x}) = \sum_{i=1}^{M} \phi_i^1 \varrho_{1,i}, \quad \varrho_2(\mathbf{x}) = \sum_{i=1}^{M} \phi_i^2 \varrho_{2,i}, \tag{54}$$

in which $\psi_i^1, \psi_i^2, \phi_i^1, \phi_i^2$ are the basis functions, N is the number of nodal displacement variables, and M is the number of nodal design variables. Linear or quadratic basis functions are used for the displacement fields and linear basis functions is used for the design fields. A regular mesh with nearly quadratic elements is used in all examples.

The discretized version of Eq. (4) with boundary conditions and PMLs is

$$\mathbf{S}(\omega)\mathbf{d} = \mathbf{f}(\omega), \tag{55}$$

where

$$\mathbf{S} = \mathbf{K} + \mathrm{i}\omega\mathbf{C} - \omega^2\mathbf{M}, \tag{56}$$

is the system matrix and $\mathbf{d} = \{u_1\ u_2 \ldots u_N \quad v_1 v_2 \ldots v_N\}^{\mathrm{T}}$ are the discretized nodal amplitudes, $\mathbf{K}$, $\mathbf{C}$ and $\mathbf{M}$ is the stiffness, damping, and mass matrices, respectively, and $\mathbf{f}$ is the frequency-dependent load vector.

The vector of design variables $\boldsymbol{\gamma} = \{\varrho_{1,1}\varrho_{1,2} \ldots \varrho_{1,M}\varrho_{2,1}\varrho_{2,2} \ldots \varrho_{2,M}\}^{\mathrm{T}}$ is introduced and the sensitivities of the objective function with respect to these design variables are obtained. Let Φ be either of the two objective functions considered and let $' = d/d\gamma_i$ denote the derivative with respect to the ith design variable. The adjoint method (e.g. Ref. [19]) leads to the expression for the derivative of the augmented objective function Φ_0:

$$\Phi_0' = \Phi' + \boldsymbol{\lambda}^{\mathrm{T}}\mathbf{R}' + \bar{\boldsymbol{\lambda}}^{\mathrm{T}}\bar{\mathbf{R}}', \tag{57}$$

where Φ' is the derivative of the objective function, $\boldsymbol{\lambda}$ is a vector of Lagrangian multipliers, and $\mathbf{R}'$ is the derivative of the residual of Eq. (55) that vanishes at equilibrium ($\mathbf{R} = \mathbf{R}' = \mathbf{0}$). Straightforward calculations lead to an equation for the Lagrangian multipliers:

$$\mathbf{S}^{\mathrm{T}}\boldsymbol{\lambda} = -\left(\frac{\partial\Phi}{\partial\mathbf{d}^r} - \mathrm{i}\frac{\partial\Phi}{\partial\mathbf{d}^i}\right)^{\mathrm{T}}, \tag{58}$$

so that the final expression for the sensitivities become:

$$\Phi' = \frac{\partial\Phi}{\partial\gamma_i} + \mathrm{Re}\left(\boldsymbol{\lambda}^{\mathrm{T}}\frac{\partial\mathbf{S}}{\partial\gamma_i}\mathbf{d}\right). \tag{59}$$

The implementation of the sensitivity analysis is facilitated by the use of the COMSOL software, that allows for an almost automated generation of the derivatives [20].

5.4. Optimization problem formulation

With artificial damping included the overall power balance can be written:

$$R = 1 - (T + D + D_{\mathrm{art}}), \tag{60}$$

where T, D and D_{art} are defined in Eqs. (51), (35) and (41). From Eq. (60) it is seen that the artificial damping reduces R so that intermediate design variables are costly and likely to be penalized from the design.

In the example in Section 6 the wave reflection is maximized. Only scattering inclusions are considered so there is no real dissipation ($D = 0$). However, if material damping is added the convergence of the

optimization algorithm is enhanced and the risk of obtaining a local optimum is reduced [2]. The material damping is applied using a continuation method in which the optimization procedure is initiated with high damping which is then gradually removed as the optimization progresses. A reverse procedure is used with the artificial damping. The optimization is started with a small (or vanishing) artificial damping coefficient β_1 which is then increased slowly.

For the second optimization problem, the power balance (60) is rewritten as:

$$D = 1 - (T + R + D_{\text{art}}), \tag{61}$$

from which it is seen that artificial damping penalizes intermediate design variables also when D is maximized.

Both optimization problems are solved with Krister Svanberg's MMA routine [21] with multiple load cases that comprise several frequencies for pressure and shear waves. The implementation is based on the min–max approach [22] and the final optimization problem is written:

$$\begin{aligned} &\min_{\boldsymbol{\gamma}} \max_{\omega_i} (\Phi_p(\omega_i),\ \Phi_s(\omega_i)) \\ \text{subject to}: \quad &\mathbf{S}(\omega_i)\mathbf{d} = \mathbf{f}(\omega_i) \\ &0 \leqslant \boldsymbol{\gamma} \leqslant 1, \end{aligned} \tag{62}$$

in which $\Phi = T + D + D_{\text{art}}$ for the reflection problem and $\Phi = 1 - D$ for the dissipation problem. The subscripts p and s refer to pressure and shear waves and ω_i is any of the frequencies that are considered. Thus, the formulation in Eq. (62) states that the maximum value of the objective function Φ for both wave types and all frequencies is to be minimized by an optimized set of design variables $\boldsymbol{\gamma}$ that fulfills the constraints.

6. Numerical example 1

In this first example the aim is to design a structure that reflects both P and S wave pulses. The wave pulse is assumed to be narrow-band with center frequency f_0 and the main frequency content in a finite frequency range near the center frequency. A possible application could be for isolation of structures from ground-borne waves, e.g. coming from underground train tunnels. The properties of the materials used in this example have been taken partly from studies of train-induced ground vibrations [23]. Table 1 lists the material properties of the three materials that are used.

The optimized design should be a compromise between having a sufficient reflection of waves but also a structure with manageable spatial dimensions. The length of the design domain slab, L, is chosen to be one wavelength for a P wave in the host material. With a center frequency of $f_0 = 788\,\text{Hz}$ this gives $L = 1\,\text{m}$.

Before optimized designs are generated the reflectance is computed for two structures with inclusions of scattering material (scatter 1) placed periodically in the design domain. It is well known that periodically placed inclusions may cause bandgaps in the corresponding band structure which leads to high reflection. This occurs if the material contrast is sufficiently high and the wavelength is commensurable with the periodicity [1].

Fig. 3a shows a one-dimensional periodic structure, a Bragg-grating, and the corresponding reflectance (Fig. 3b). Large frequency bands with high reflectance exist for pressure and shear waves, but they are off-set due to the difference in wavelength. However, near the center frequency $f_0 = 788\,\text{Hz}$ high reflectance occurs for both wave types. For the two-dimensional periodic structure (Fig. 4a) frequency bands with high

Table 1
Material properties used for the reflection example

Material	ρ (kg/m^3)	E (MPa)	ν	η_ρ (s^{-1})
Host (ground)	1550	269	0.257	—
Scatter 1 (ground)	2450	2040	0.179	—
Scatter 2	775	134.5	0.257	—

The material data for the two ground types is taken from Ref. [23].

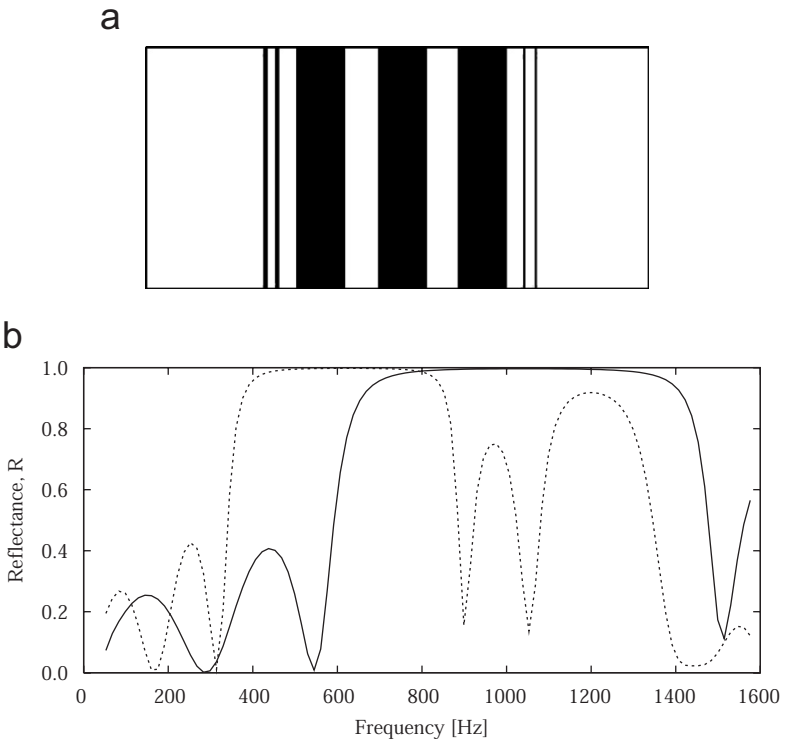

Fig. 3. (a) One-dimensional periodic structure (Bragg grating) with three inclusions of scatter 1 (black) in the host ground material (white); (b) the corresponding reflected power R for P and S waves. P wave (solid line), S wave (dashed line).

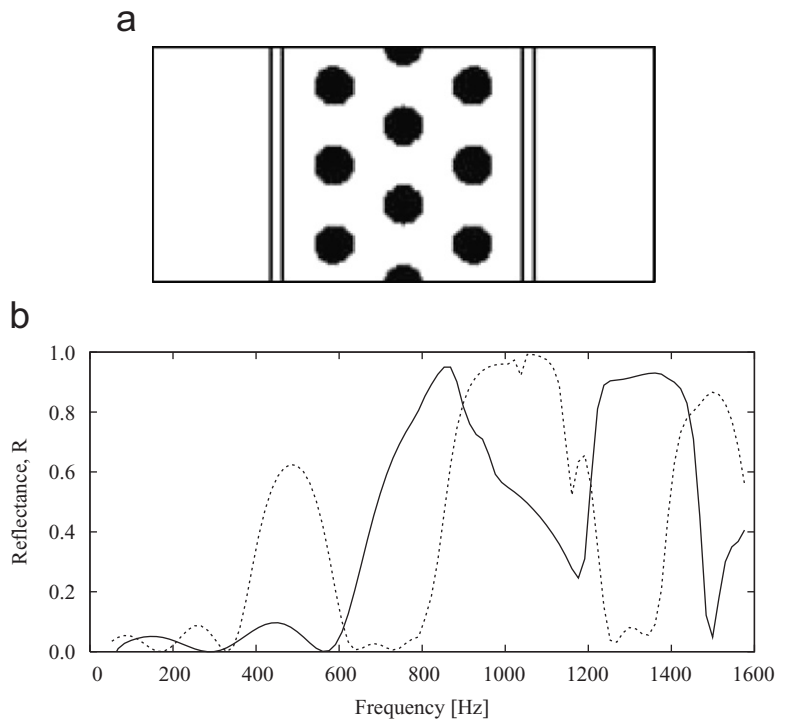

Fig. 4. (a) Two-dimensional triangular periodic structure with three rows of scatter 1 inclusions (black) in the host ground material (white); (b) the corresponding reflected power R for P and S waves. P wave (solid line), S wave (dashed line).

reflectance are also seen (Fig. 4b) but the reflectance is generally lower than for a Bragg-grating with the same number of rows of inclusions. However, a 2D-structure is known better to reflect waves from different angles of incidence [1]. The size of the inclusions were chosen after a simple parameter study so that a large reflectance was obtained near $f_0 = 788$ Hz. It should be emphasized that a further improvement is possible by using repetitive cells with an optimized material distribution [2]. However, the improvement that can be obtained with further cell optimization is small due to the restricted design space.

6.1. Two-phase design

Thus, with two materials available a one-dimensional layered structure seems a good candidate as an optimal design. However, as will be shown in this section this depends on whether the frequency range is sufficiently small so that high reflectance bands for P and S waves can overlap. First the optimization is performed for a relative small frequency range ±10% away from the center frequency. Fig. 5 shows the optimized design and the reflectance curves for pressure and shear waves. The design is a one-dimensional structure with three inclusion layers of different thickness and with uneven spacing between them. Everywhere in the target frequency range a high reflectance is obtained.

The target frequency range is now extended to ±25% and Fig. 6a shows the optimized design (with 10 optimization frequencies in the target range). The design is no longer a one-dimensional layered structure since such a structure cannot reflect both wave types sufficiently in the entire frequency range. Instead a combination of a layered structure and a more intricate 2D material arrangement is seen. Fig. 6b shows that the reflectance is more than 90% in the entire optimization range. Fig. 7 shows the corresponding wave pattern for P and S waves at the center frequency and illustrates how wave amplitudes are attenuated in the structure.

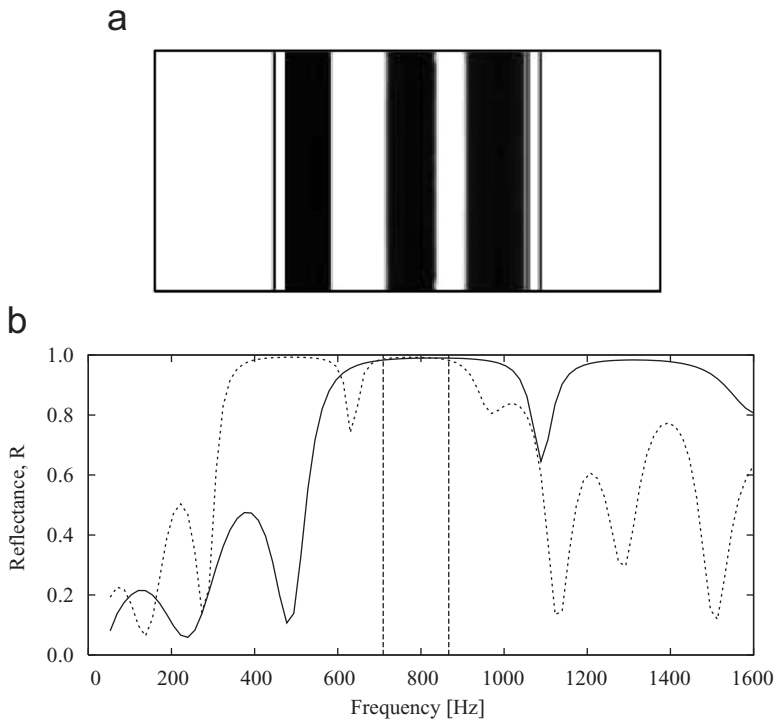

Fig. 5. (a) Optimized distribution of scatter 1 (black) and host material (white) for maximum reflectance in a ±10% frequency interval around the center frequency $f_0 = 788$ Hz; (b) resulting reflectance curves for P and S waves. P wave (solid line), S wave (dashed line).

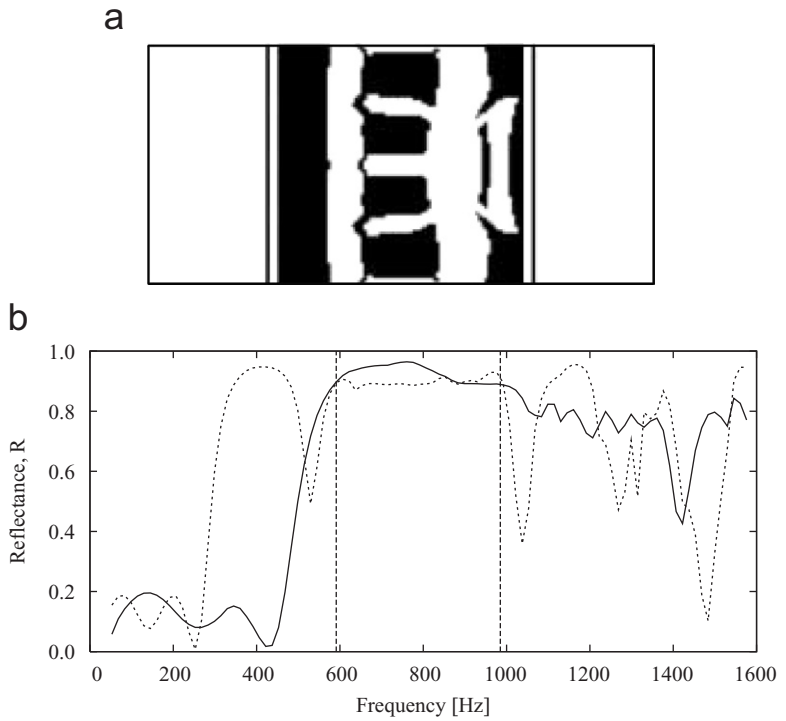

Fig. 6. (a) Optimized distribution of scatter 1 (black) and host material (white) for maximum reflectance in a ±25% frequency interval around the center frequency $f_0 = 788$ Hz; (b) resulting reflectance curves for P and S waves. P wave (solid line), S wave (dashed line).

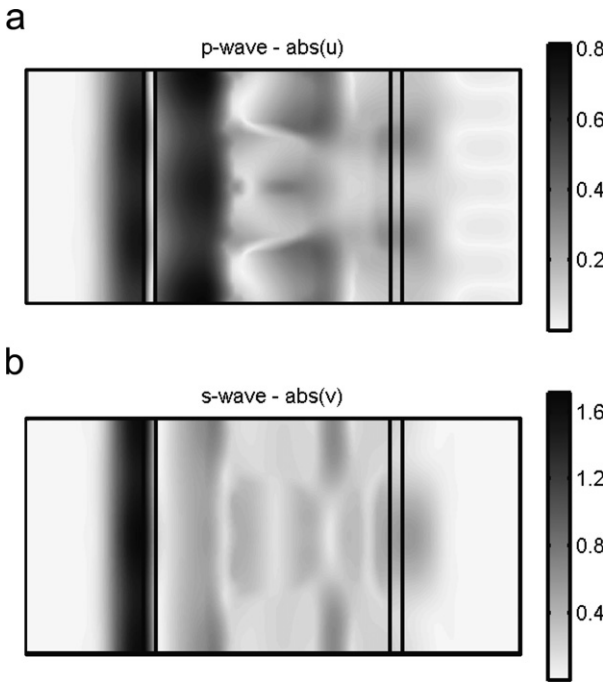

Fig. 7. Wave patterns for the optimized structure computed for the center frequency $f_0 = 788$ Hz: (a) abs(u) for a P wave and (b) abs(v) for an S wave.

It should be emphasized that other local optima can be found with different initial material distributions. The design shown in Fig. 6a is the best structure found after an extensive search but it is not guaranteed to be the global optimum. The problem with many local optima in wave-propagation problems is known and has to the author's knowledge not yet been solved. Genetic or other evolutionary algorithms are not easily applied to this problem due to the large number of design variables (5000 or more).

6.2. Three-phase design

A more effective wave-reflecting structure can be obtained if the design domain length L is increased. This allows for more inclusion layers in the structure and consequently higher reflectance. Also for larger L the optimized design has a combined layered/2D appearance (as in Fig. 6a) so that it is effective in the entire frequency range.

For situations where the spatial extent of the design domain is limited higher reflectance can be obtained with increased contrast between the inclusion material and the host. This contrast can be quantified as the ratio between the impedances (cf. Eq. (26)–(27)). Generally, the layout of the optimized designs is different for different contrasts.

However, an additional scattering material does not seem to increase the reflectance. Extensive numerical experiments showed in all cases that a design with those two materials having the highest contrast is always better than a three-phase design. This supports previous studies that indicate that maximum contrast is favorable for high wave reflection (cf. Section 4.1).

Fig. 8 illustrates this effect. A third material phase is introduced (Table 1) and the corresponding optimized design (Fig. 8a) consists mainly of scatter 1 (gray) and scatter 2 (black) as they have the largest material contrast. However, small areas of host material (white) are seen in the design. If these areas are replaced by scattering material (Fig. 8b), the reflectance (Fig. 8c) is almost identical as for the optimized 3-phase design and actually slightly better averaged over the target range. Thus, it can be concluded that the 3-phase optimized design is a local optimum.

Quadratic elements were used for the displacement fields in the last example to increase the convergence and stability of the optimization algorithm. However, although an improvement was noted the final design is still unsymmetrical which is an indication of the instabilities in the optimization procedure. The design is also dominated by small fragmented details. To remedy this problem, different filtering techniques could be applied (e.g. Ref. [15]). This has not been examined further in this work.

7. Numerical example 2

In this second example the setting from the first example is kept but now the goal is to maximize the fraction of the input power that is dissipated in the slab. An absorptive material phase with the properties of epoxy (Table 2) is introduced. The damping coefficient is chosen arbitrarily as $\eta_\rho = 0.05\,\mathrm{s}^{-1}$ and the damping of the other material phases is neglected. The importance of η_ρ will be investigated for the optimized designs. A third material phase (scatter) is also introduced and it will be investigated how this can improve the performance of the design. The material properties of this material are chosen so that the density is twice and the stiffness 20 times that of the host material.

The dissipated power fraction D is computed for the situation with the entire design domain filled up with absorptive material. Fig. 9 shows the dissipation of a P and an S wave with $\eta_\rho = 0.05\,\mathrm{s}^{-1}$ and also for higher values of η_ρ. Due to the impedance contrast between the two material phases a part of the incident wave is reflected directly at the input boundary and consequently not all input power is dissipated regardless of the magnitude of η_ρ.

Thus, merely filling up the domain with absorptive material is not optimal for maximum dissipation, although perhaps intuitively attractive. Instead, a good design must ensure a low direct reflection at the input boundary and additionally ensure that the wave is not transmitted but reflected inside the domain and then dissipated. The following sections demonstrate that such designs are generated by the optimization algorithm.

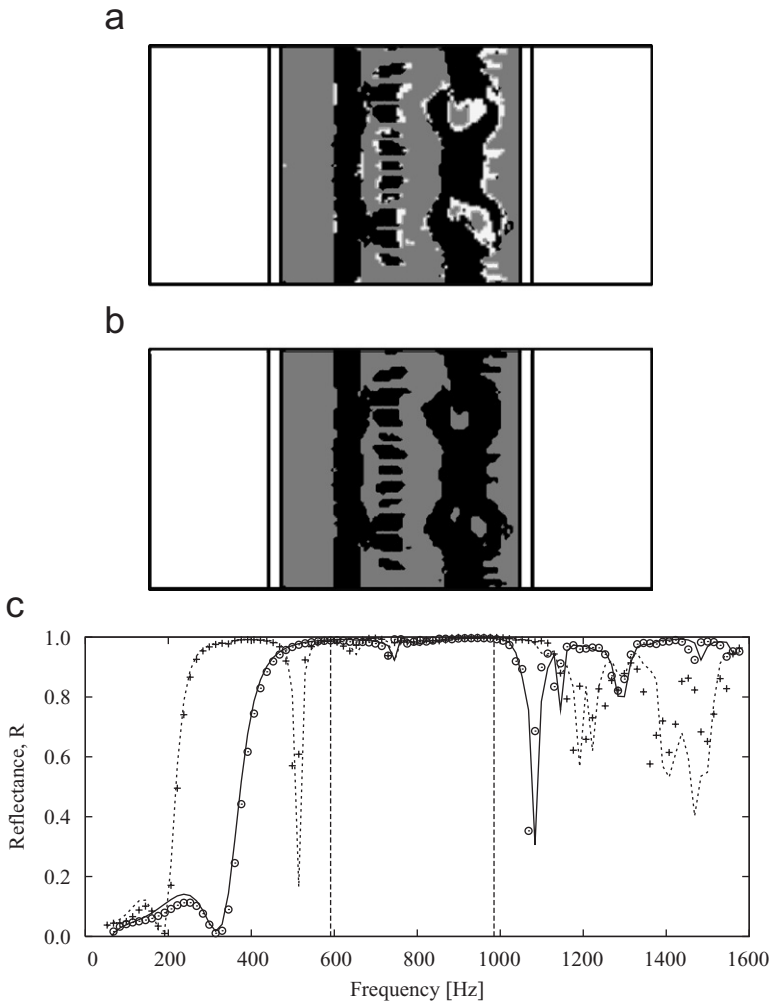

Fig. 8. (a) Optimized distribution of scatter 1 (gray), scatter 2 (black) and host (white); (b) 2-phase design with host replaced by scattering material; (c) resulting reflectance curves for P and S waves. P wave (solid line), S wave (dashed line), P wave-2 phase (discrete circles), S wave-2 phase (discrete crosses).

Table 2
Material properties for the materials used in the dissipation example

Material	ρ (kg/m^3)	E (MPa)	v	η_ρ (s^{-1})
Host (ground)	1550	269	0.257	—
Epoxy	2000	4000	0.400	0.05
Scatter	3100	5380	0.350	—

The material data for the ground is taken from Ref. [23].

7.1. Two-phase design

In this section host and the absorptive material are used for the optimization. Fig. 10a shows an optimized design for shear and pressure waves in a $\pm 10\%$ frequency range near the center frequency with 10 optimization frequencies used. The optimized design is complicated but with characteristic features. A thin

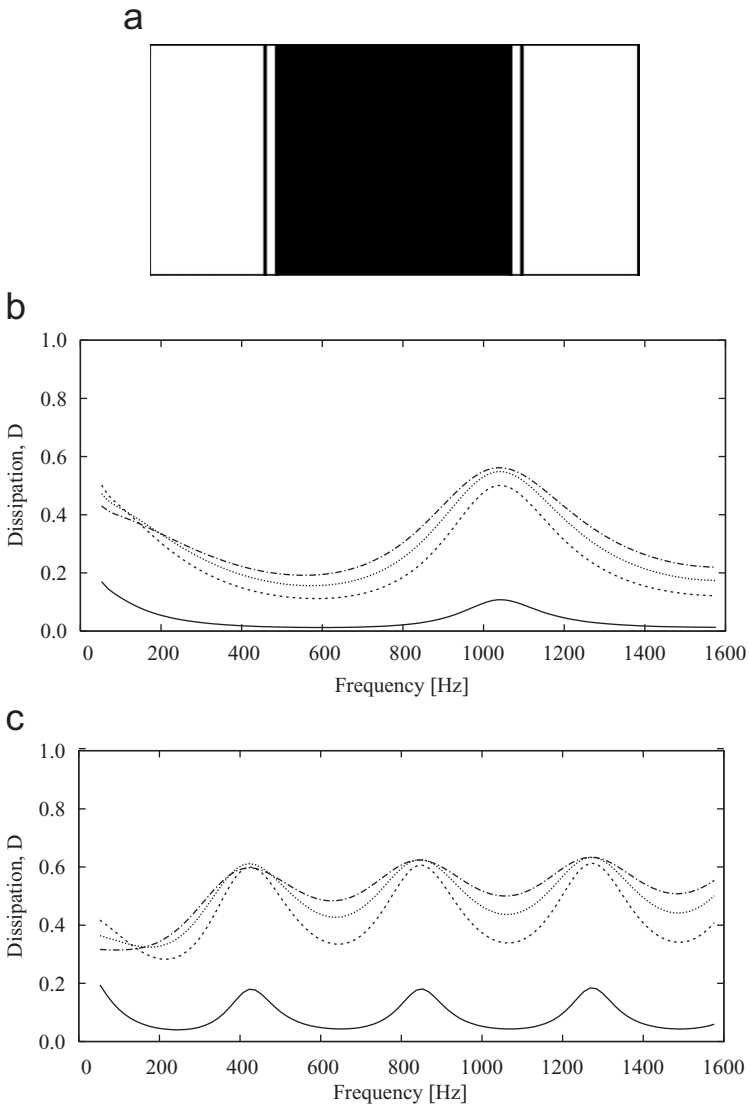

Fig. 9. (a) Design domain filled with absorptive material (epoxy), corresponding dissipated energy fraction D for (b) P and (c) S waves for four different values of η_ρ. $\eta_\rho = 0.05\,\mathrm{s}^{-1}$ (solid), $\eta_\rho = 0.50\,\mathrm{s}^{-1}$ (dash), $\eta_\rho = 0.75\,\mathrm{s}^{-1}$ (dot), $\eta_\rho = 1.00\,\mathrm{s}^{-1}$ (dash–dot).

inclusion slab at the input boundary modifies the effective impedance seen by the incident wave so that the direct reflection is minimized. The thicker slab at the output boundary maximizes the reflection of the wave that "escapes" through the domain. The inner parts of the domain are filled with strategically placed inclusions that dissipate the high amplitude waves.

Fig. 10b shows curves for the dissipated power fraction. The dissipation is significantly increased in the target range and is a factor 2–10 higher than for the case with the whole domain filled (Fig. 9). The dissipation is also plotted for the same structure with a higher value of η_ρ. It is noted that the dissipation approaches unity. This implies that the structure effectively reduces the direct reflection and the transmission through the domain to a minimum. This also indicates that the specific choice of η_ρ used in the optimization algorithm is not critical for the generation of the optimized design. Fig. 11 shows the point-wise distribution of the dissipated power for the two wave types computed at the center frequency. The dissipation of both wave types is seen to be localized and concentrated in a few absorptive inclusions near the input boundary and in the inner part of the domain.

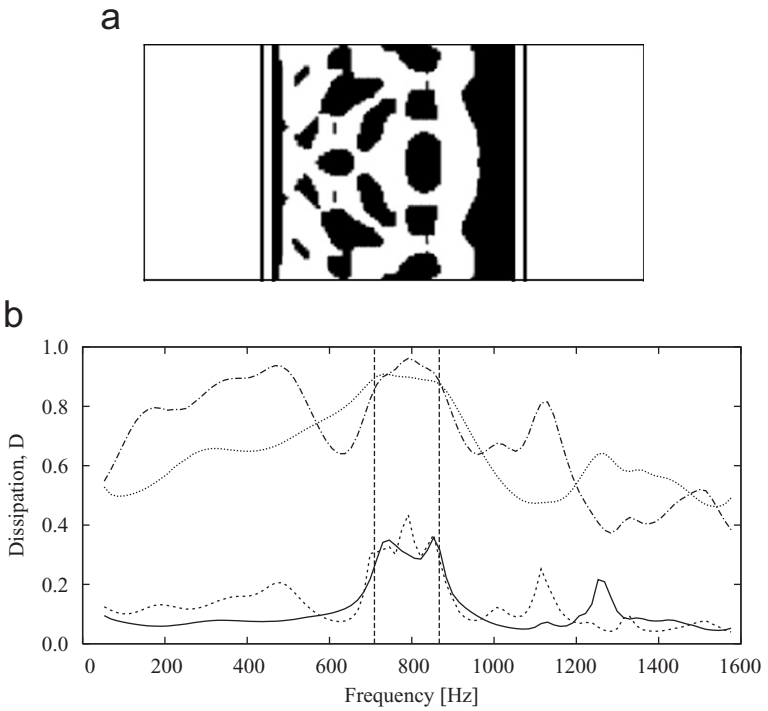

Fig. 10. (a) Optimized distribution of absorptive material (black) and loss-free host material (white) for maximum dissipation in a ±10% frequency interval around $f_0 = 788$ Hz; (b) corresponding dissipation of P and S waves. P wave $\eta_\rho = 0.05\,\mathrm{s}^{-1}$ (solid), S wave $\eta_\rho = 0.05\,\mathrm{s}^{-1}$ (dash), P wave $\eta_\rho = 0.75\,\mathrm{s}^{-1}$ (dot), S wave $\eta_\rho = 0.75\,\mathrm{s}^{-1}$ (dash–dot).

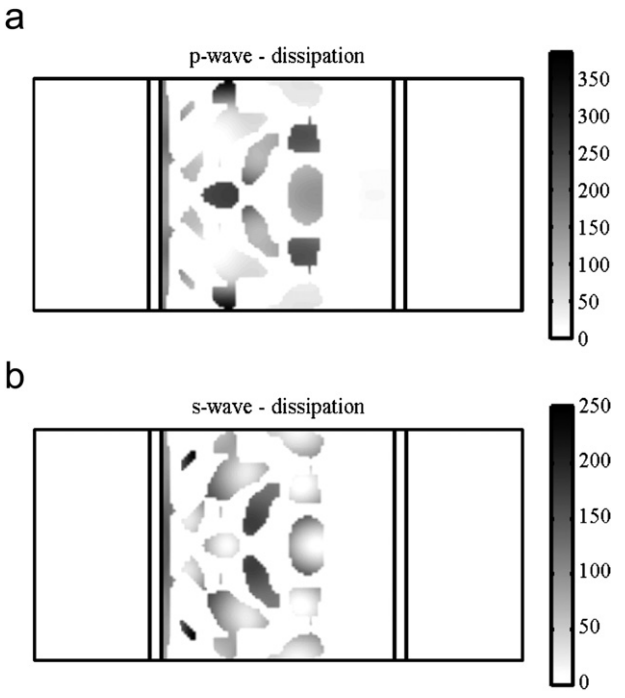

Fig. 11. Point-wise dissipated power for the optimized design for $f_0 = 788$ Hz: (a) a P wave and (b) an S wave. $\eta_\rho = 0.05\,\mathrm{s}^{-1}$.

7.2. Three-phase design

The extra scattering material is now included in an attempt to further improve the performance. The hypothesis is that with a highly reflecting material available a larger part of the wave can be reflected leading to higher wave amplitudes and higher dissipation. Fig. 12a shows the optimized design with gray as absorptive material and black as scattering material. Qualitatively, the design is similar to the two-phase design. The major difference is that the inclusion near the output boundary is made of the scattering material as the higher impedance contrast leads to increased reflection. Additionally, two small reflecting inclusions are seen in the inner part of the structure.

Fig. 12b shows the dissipated power fraction for the three-phase design. The improvement of the performance is quite limited (from about 32% to about 35% in average) and although the details of the two-phase and three-phase designs are different the performance in the target range is similar. Thus, it seems possible to create many good optimized designs (local optima) with similar overall features but with different structural details such as precise size and placement of the absorptive inclusions.

The effect of a refinement of the computational model and the use of higher-order finite elements is illustrated in Fig. 13. Fig. 13a shows the optimized design with quadratic elements for the displacement fields instead of linear elements. The higher-order elements stabilize the optimization algorithm (as for the reflection example) and the small asymmetries in the design in Fig. 12a vanish. Apart from this the two designs are very similar. Fig. 13b shows an optimized design with 100×100 linear elements in the design domain (80×80 used in the other examples) and with 15 optimization frequencies in the target range (instead of 10 used in the other examples). The overall features of the design are unchanged but the details are different. The numerical instabilities are more severe and lead to a very unsymmetrical design. However, as illustrated in Fig. 13c, these differences in the design are not reflected in the performance which is very similar in the target range.

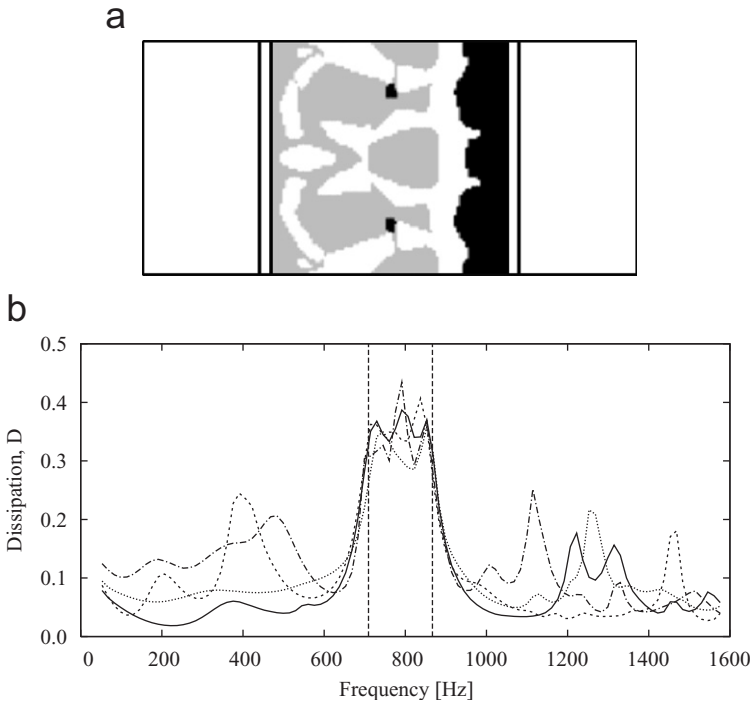

Fig. 12. (a) Optimized distribution of absorptive material (gray), host material (white), and scattering material (black) for maximum dissipation in a $\pm 10\%$ frequency interval around $f_0 = 788$ Hz; (b) corresponding dissipation of P and S waves compared to the two-phase design in Fig. 10. P wave-3 phase (solid), S wave-3 phase (dash), P wave-2 phase (dot), S wave-2 phase (dash–dot). $\eta_p = 0.05\,\mathrm{s}^{-1}$.

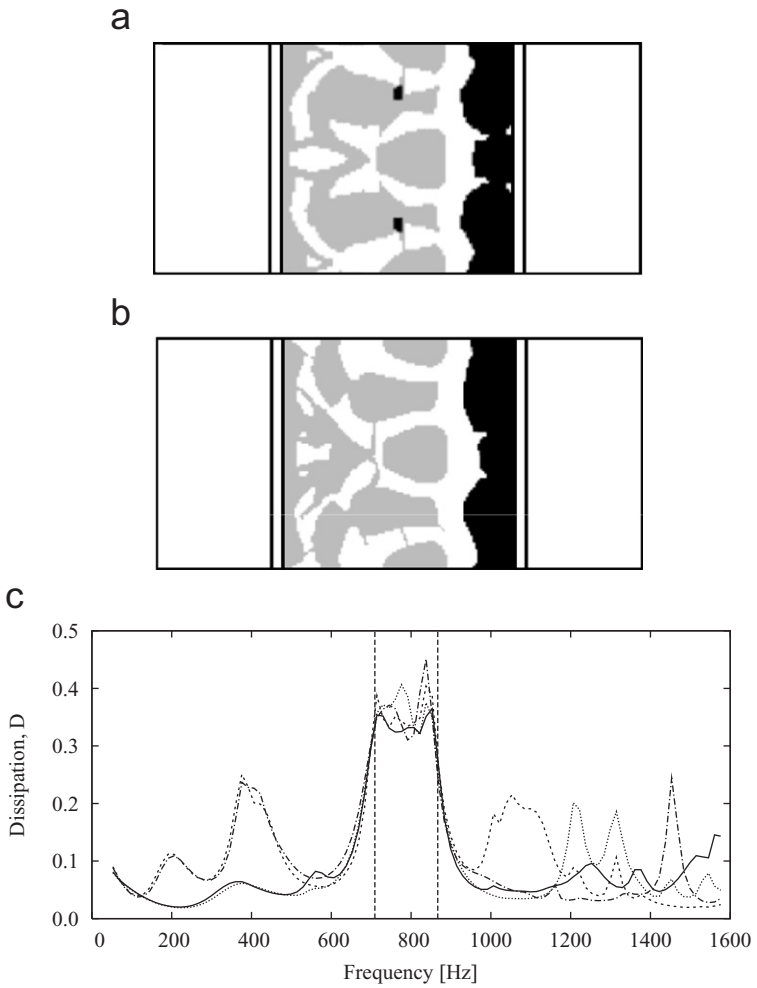

Fig. 13. (a) Optimized design obtained with quadratic elements for the displacement amplitudes; (b) design obtained with refined mesh and more optimization frequencies in the target range; (c) the corresponding dissipation for P and S waves. P wave-refined (solid), S wave-refined (dash), P wave-quadratic (dot), S wave-quadratic (dash–dot). $\eta_\rho = 0.05\,\mathrm{s}^{-1}$.

Fig. 14 shows the point-wise dissipated power computed at the center frequency for the structure generated with quadratic elements for the displacement fields. The dissipation is fairly well distributed for the P wave and more localized near the input boundary for the S wave. The behavior of the optimized absorptive structure is further examined in Fig. 15. The dissipation (D), reflectance (R), and transmittance (T) are depicted for an S wave. As seen in Fig. 15a ($\eta_\rho = 0.05\,\mathrm{s}^{-1}$) the increase in dissipation in the target range is accompanied by a large drop in R. However, the transmission T is relatively large due to the small dissipation in the absorptive inclusions. If a material with a larger damping coefficient is used ($\eta_\rho = 0.75\,\mathrm{s}^{-1}$) the reflection R is again very small, but now almost all of the wave that propagates through the structure is dissipated and consequently the transmission T of the wave is almost reduced to zero. Similar behavior is seen for a P wave.

8. Conclusions

Two topology optimization problems for elastic wave propagation were considered. The objective of the optimization study was to optimize the distribution of two or three material phases in a slab of material so that

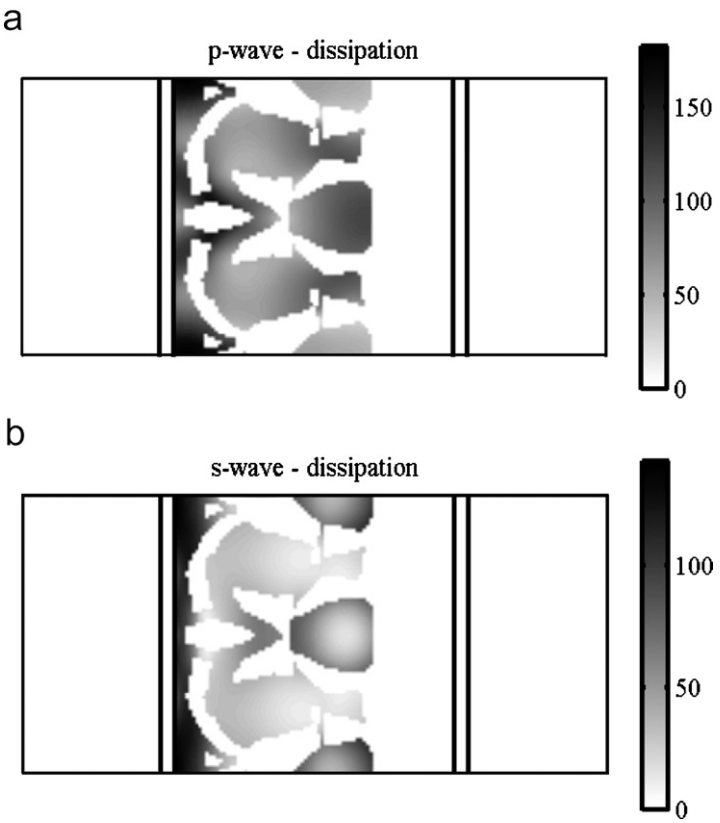

Fig. 14. Point-wise dissipated power for the optimized design for $f_0 = 788\,\text{Hz}$: (a) a P wave and (b) an S wave. $\eta_\rho = 0.05\,\text{s}^{-1}$.

wave propagation was hindered. This was accomplished either by maximizing the reflection from the slab or the wave dissipation in the slab.

A design domain was defined and parameterized with two continuous design fields that control the material properties. With two design fields up to three different material phases could be distributed in the domain. A penalization method based on artificial damping was introduced. The penalization was employed to ensure well-defined material properties in the final design.

The optimization problems were formulated and discretized with a standard finite element method and implemented with the commercial software COMSOL. The optimization problem was solved with the aid of the mathematical programming software MMA, with analytical sensitivity analysis and a min-max formulation so that pressure and shear waves for multiple wave frequencies could be considered.

The use of the optimization algorithm was demonstrated by two application examples. The propagation of a ground-borne wave pulse was suppressed by optimizing the material distribution in a square design domain. In the first example scattering inclusions were distributed to maximize the wave reflection and in the second example the wave dissipation was maximized with an optimized distribution of absorbing and scattering inclusions.

The examples have demonstrated that large reflection of waves can be obtained by optimizing the distribution of two material phases but also that adding a third phase with intermediate material properties could not lead to further improvement. By optimizing the distribution of absorbing material the dissipation of waves can be significantly enhanced and it was shown that the dissipation could be further increased by including also a scattering material phase in the design optimization.

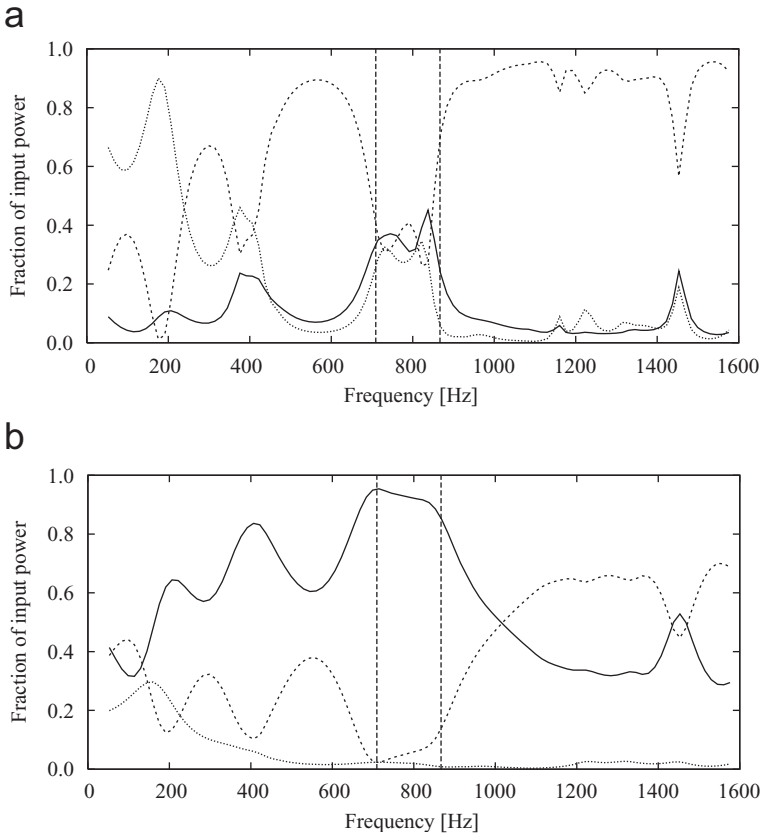

Fig. 15. Dissipation D, reflectance R, and transmittance T for the optimized three-phase design in Fig. 13a for an S wave, (a) $\eta_\rho = 0.05\,\mathrm{s}^{-1}$ and (b) $\eta_\rho = 0.75\,\mathrm{s}^{-1}$. Dissipation (solid), reflectance (dash), transmittance (dot).

Acknowledgements

The work was partially supported by the Danish Technical Research Council through the project "Designing bandgap materials and structures with optimized dynamic properties" and by the Danish Center for Scientific Computing (DCSC).

References

[1] M. Sigalas, M.S. Kushwaha, E.N. Economou, M. Kafesaki, I.E. Psarobas, W. Steurer, Classical vibrational modes in phononic lattices: theory and experiment, *Zeitschrift für Kristallographie* 220 (2005) 765–809.

[2] O. Sigmund, J.S. Jensen, Systematic design of phononic band-gap materials and structures by topology optimization, *Philosophical Transactions of the Royal Society London, Series A (Mathematical Physical and Engineering Sciences)* 361 (2003) 1001–1019.

[3] C. Rupp, M. Frenzel, A. Evgrafov, K. Maute, M.L. Dunn, Design of nanostructures phononic materials, *Proceedings of IMECE2005, 2005 ASME International Mechanical Engineering Congress and Exposition*, Orlando, Florida, USA, 2005.

[4] S. Halkjær, O. Sigmund, J.S. Jensen, Inverse design of phononic crystals by topology optimization, *Zeitschrift für Kristallographie* 220 (2005) 895–905.

[5] M.I. Hussein, K. Hamza, G.M. Hulbert, R.A. Scott, K. Saitou, Multiobjective evolutionary optimization of periodic layered materials for desired wave dispersion characteristics, *Structural and Multidisciplinary Optimization* 31 (2006) 60–75.

[6] J.S. Jensen, Optimal design of lossy bandgap structures, *Proceedings of XXI International Congress on Theoretical and Applied Mechanics*, pages on CD–rom, Warsaw, August 15–21, 2004.

[7] D. Razansky, P.D. Einziger, D.R. Adam, Effectiveness of acoustic power dissipation in lossy layers, *Journal of the Acoustic Society of America* 116 (1) (2004) 84–89.

[8] I. Takewaki, Optimal damper placement for planar building frames using transfer functions, *Structural and Multidisciplinary Optimization* 20 (2000) 280–287.

[9] J.A. Bishop, A.G. Striz, On using genetic algorithms for optimum damper placement in space trusses, *Structural and Multidisciplinary Optimization* 28 (2004) 136–145.
[10] C.S. Jog, Topology design of structures subjected to periodic loading, *Journal of Sound and Vibration* 253 (3) (2002) 687–709.
[11] B. Wang, G. Chen, Design of cellular structures for optimum efficiency of heat dissipation, *Structural and Multidisciplinary Optimization* 30 (2005) 447–458.
[12] S.J. Cox, D.C. Dobson, Maximizing band gaps in two-dimensional photonic crystals, *SIAM Journal for Applied Mathematics* 59 (6) (1999) 2108–2120 ISSN 00361399.
[13] J.S. Jensen, O. Sigmund, Systematic design of photonic crystal structures using topology optimization: low-loss waveguide bends, *Applied Physics Letters* 84 (12) (2004) 2022–2024.
[14] D. Royer, E. Dieulesaint, *Elastic Waves in Solids I*, Springer, Berlin, Heidelberg, 2000 ISBN 3-540-65932-3.
[15] M.P. Bendsøe, O. Sigmund, *Topology Optimization—Theory, Methods and Applications*, Springer, Berlin, Heidelberg, 2003.
[16] J.S. Jensen, O. Sigmund, Topology optimization of photonic crystal structures: a high-bandwidth low-loss T-junction waveguide, *Journal of the Optical Society of America B* 22 (6) (2005) 1191–1198.
[17] G. Allaire, G.A. Francfort, A numerical algorithm for topology and shape optimization, in: M.P. Bendsøe, C.A. Mota Soares (Eds.), *Topology Optimization of Structures*, Klüwer Academic Publishers, Dordrecht, 1993, pp. 239–248.
[18] U. Basu, A.K. Chopra, Perfectly matched layers for time-harmonic elastodynamics of unbounded domains: theory and finite-element implementation, *Computer Methods in Applied Mechanics and Engineering* 192 (2003) 1337–1375.
[19] D.A. Tortorelli, P. Michaleris, Design sensitivity analysis: overview and review, *Inverse Problems in Engineering* 1 (1994) 71–105.
[20] L.H. Olesen, F. Okkels, H. Bruus, A high-level programming-language implementation of topology optimization applied to steady-state navier-stokes flow, *International Journal for Numerical Methods in Engineering* 65 (2006) 975–1001.
[21] K. Svanberg, The method of moving asymptotes—a new method for structural optimization, *International Journal for Numerical Methods in Engineering* 24 (1987) 359–373.
[22] K. Svanberg, The method of moving asymptotes—modelling aspects and solution schemes, Lecture Notes for the DCAMM Course: advanced Topics in Structural Optimization, Lyngby, June 25–July 3, 1998.
[23] D.V. Jones, M. Petyt, Ground vibration in the vicinity of a strip load: an elastic layer on an elastic half-space, *Journal of Sound and Vibration* 161 (1) (1993) 1–18.